



# Interdecadal variations and causes of the relationship between the winter East Asian monsoon and interhemispheric atmospheric mass oscillation

Chuhan Lu<sup>1,2</sup> · Lei Zhong<sup>2</sup> · Zhaoyong Guan<sup>2</sup> · Nian Qiao<sup>2</sup>

Received: 28 November 2022 / Accepted: 25 April 2023 / Published online: 8 May 2023  
© The Author(s), under exclusive licence to Springer-Verlag GmbH Germany, part of Springer Nature 2023

## Abstract

The East Asian winter monsoon (EAWM) intensifies in the early twenty-first century and links with frequent impacts of large-scale persistent extreme cold events in winter in East Asia in recent years. We found that there has been a significant positive correlation between the EAWM and Interhemispheric Oscillation (IHO). However, conspicuous interdecadal variations have occurred in the relationship between the EAWM and IHO. The relationship between the IHO and EAWM was most significant during 1979–2020, but this relationship was weak and insignificant during 1962–1978. During 1979–2020, the atmospheric mass (surface pressure) difference between the Northern Hemisphere (NH) and Southern Hemisphere (SH) during 1979–2020 was significantly reduced by 7.85% ( $0.75 \times 10^{15}$  kg) compared with that during 1962–1978. Such interhemispheric redistribution of atmospheric mass (AM) has had a distinct impact on the land-sea pressure contrast in East Asia and has intensified the connection between the EAWM and IHO. A strengthened EAWM has resulted in notable cooling and more severe winters in China. The apparent exportation of AM in the Antarctic region is an important driving factor for this interhemispheric change. The accompanying anomalous accumulation of AM in the NH is linked with an increase in the pressure difference between land and sea in East Asia, resulting in intensifying correlation between IHO and the EAWM. The decadal enhancement of the IHO during 1979–2020 was closely connected with conspicuous warming in the tropical troposphere/lower stratosphere (UTLS). A seesaw pattern of anomalous air temperature and ozone between tropical and Antarctic UTLS has induced a decrease in Antarctic ozone masses and air temperature and has strengthened the polar vortex, corresponding to a decadal enhancement of interhemispheric AM imbalance.

**Keywords** Interhemispheric oscillation · East Asian winter monsoon · Extreme low-temperature events · Polar vortex

## 1 Introduction

The East Asian Winter Monsoon (EAWM) is an important part of the East Asian atmospheric circulation system and has a wide influence on East Asian weather and climate (He et al. 2007). Previous studies have shown that the EAWM plays an important leading role in East Asian winter temperature variation, and has a direct and substantial influence

on winter surface temperature (SAT) variation in China (Hu 2015). Ma and Chen (2021) pointed out that interdecadal variations of winter temperature in China were closely related to EAWM. On the decadal time scale, EAWM has undergone two significant decadal changes since the mid-twentieth century to the present, one in the mid-1980s (from strong to weak) and the other in the early 2000s (from weak to strong). Related to this change in EAWM, winter temperatures across China have experienced similar interdecadal fluctuations. From the late 1980s to the early 2000s, temperatures were generally higher in East Asia and China as the decadal weakening of EAWM occurred, and China experienced many mild winters. However, with the strengthening of the East Asian winter monsoon in the early twenty-first century, large-scale persistent extreme cold events occurred frequently in the mid-latitudes of the Northern Hemisphere (NH), especially in East Asia (e.g., Jeong et al. 2011; Wu

✉ Chuhan Lu  
luchuhan@nuist.edu.cn

<sup>1</sup> Key Laboratory of Ecosystem Carbon Source and Sink, China Meteorological Administration (ECSS-CMA), Wuxi University, wuxi 214063, China

<sup>2</sup> Key Laboratory of Meteorological Disaster, Ministry of Education, Nanjing University of Information Science and Technology, 210044, Nanjing, China

et al. 2011, Lu 2016). For example, a strengthening Siberian high and EAWM induced by cold advection by northerly led to widespread snow and rain freezing in central and eastern China in January 2018 (Sun et al. 2019). In addition, the intensity of EAWM can also affect the outbreak of the South China Sea Summer Monsoon, and thus exert an important influence on summer temperature and precipitation in China (You et al. 2021). Therefore, the study of EAWM is one of the keys to understanding the mechanism of climate change in East Asia.

Previous studies have shown that the low frequency variation of EAWM is closely related to the large scale circulation background in the NH. Internal variables, such as the Pacific Decadal Oscillation (PDO) and Arctic oscillation (AO), are important factors influencing decadal scale EAWM (Gong 2019; Chen et al. 2019a, b). The analysis of Zhou et al. (2007) showed that there was a significant negative correlation between PDO and EAWM. Specifically, PDO was essentially in a warm period from the mid to late 1970s until the end of the twentieth century, and EAWM was weaker during this period. Chen et al. (2005) pointed out that interdecadal variation of EAWM is closely related to AO. Positive AO position corresponds to weak EAWM and vice versa. On the interannual time scale, the different positions of the AO correspond to the different states of the polar night jet, which will change the propagation and amplitude of quasi-steady planetary waves in the atmosphere, leading to a change in the intensity of the Siberian high and the interannual variation in EAWM intensity (Chen et al. 2005; Wang et al. 2009). Other large-scale atmospheric signals, such as the North Atlantic Oscillation, midlatitude wave train and the intraseasonal oscillation of the tropical atmosphere, also play important roles in the seasonal, interannual and interdecadal changes in the EAWM (e.g., Sung 2010, Yao et al. 2016, Lim Kim 2016, Song and Wu 2017, 2019). In addition, the external forcing factors of ocean, land surface, ice and snow, such as the North Atlantic SSTA, El Niño, the change in snow cover in the middle and high latitudes of Eurasia and Arctic sea ice, are also the key driving factors of the EAWM (Wu 2011, Chen et al. 2014, 2019a, b, Luo 2019). The anthropogenic and natural forces also closely connect with the interdecadal changes of EAWM cannot be ignored. For example, increasing greenhouse gas concentration plays an important role in inducing interdecadal monsoons interdecadal changes in the mid-1980s by weakening East Asian trough (Miao et al. 2018).

The EAWM is mainly driven by the heat contrast between land and sea, and it is deeply affected by global climate change (Ding et al. 2014). Zeng and Li (2002) pointed out that the interaction between the NH and Southern Hemisphere (SH) is the fundamental cause of the monsoon phenomenon. In this sense, the EAWM not only plays an important role in climate change in Asia but is also linked with

cross-equatorial airflow and interhemispheric interactions. However, previous studies on the EAWM were mainly limited to the interactions of atmospheric circulation systems within the NH. It is also important to analyse the variation in the EAWM from a global perspective. Guan and Yamagata (2001) found that there are atmospheric mass (AM) oscillations between the NH and SH on multiple timescales (hereafter named interhemispheric oscillation, IHO), which indicates atmospheric interactions between the NH and SH. Lu et al. (2013) further showed that the IHO is closely related to the EAWM. That is, the IHO-associated pressure difference between the NH and SH is closely linked with meridional atmospheric transport and large-scale AM redistribution, which could induce a notable land-sea pressure gradient over East Asia and thus affect the winter monsoon activity.

Recent studies have revealed that the EAWM has significantly increased in the interdecadal period in the past ten years, which is driven by factors such as the increase in winter-blocking frequency in the Urals and the decrease in autumn sea ice in the Arctic (Wang and Chen 2014a, b; Yang and Wu 2013; Chen et al. 2019a, b). On the other hand, the global temperature has increased sharply since 1979, and this warming has obvious asymmetric characteristics between the NH and SH (Jones et al. 1999), which may further increase the interhemispheric AM contrast between the NH and SH. Under this background, there are several questions to answer: whether the relationship between the EAWM and IHO is stable, whether the interdecadal enhancement of the EAWM is regulated by the IHO-associated interhemispheric AM imbalance and redistribution, and what are the possible formation mechanisms? To answer the above questions, this paper explores the interdecadal changes in the relationship between the IHO and EAWM under the background of global warming and its influence on the change in winter low-temperature disaster events in China.

## 2 Data and methodology

The data in this paper are taken from the ERA5 analysis dataset of the European Centre for Medium-Range Weather Forecasts. The variables used are surface pressure (Ps), 10 m winds (u and v), geopotential heights, 2 m temperature, monthly average ozone mass mixing ratio and hourly 2 m temperature over a grid mesh of  $2.5^\circ \times 2.5^\circ$ . The study timeframe covers 1962–2021, and the winter of a certain year is defined as December of that year to February of the next year. In addition, the gridded dataset (CN05.1) with a  $0.25^\circ \times 0.25^\circ$  latitude and longitude resolution of surface temperature in China at the same time period is taken (Gao 2013). The monthly zonal average data of ozone detected by the OSIRIS satellite of the SPARC data plan from 2004 to 2016 (Hegglin et al. 2020)

and the monthly average data of RAOBCORE/RICH high-altitude satellite observations in the same period (Haimberger et al. 2012) are taken with a horizontal resolution of  $10^\circ \times 10^\circ$ . In this paper, the index of EAWM intensity ( $I_{EAWM}$ ) is characterized by the opposite number of the normalized mean of area averaged over 10 m meridional wind ( $v$ ) in the midlatitude ( $25^\circ\text{--}40^\circ$  N,  $120^\circ\text{--}140^\circ$  E) and low-high latitude ( $10^\circ\text{--}25^\circ$  N,  $110^\circ\text{--}130^\circ$  E) (Chen et al. 2000). The IHO index ( $I_{IHO}$ ) is constructed by using the difference between the AM of the NH and SH that represent an imbalance of AM between the NH and SH. The formula is shown in (1),

$$\left. \begin{aligned} m_{NH} &= \frac{2\pi a^2 f_D}{g_0} \int_0^{\frac{\pi}{2}} \overline{P_s(\varphi)} \cos\varphi d\varphi \\ m_{SH} &= \frac{2\pi a^2 f_D}{g_0} \int_{-\frac{\pi}{2}}^0 \overline{P_s(\varphi)} \cos\varphi d\varphi \\ I_{IHO} &= m_{NH} - m_{SH} \end{aligned} \right\} \quad (1)$$

where  $f_D = 1.0020$  is the Earth deformation parameter,  $\varphi$  is the latitude, and  $\overline{P_s}$  is the zonal mean surface pressure.

### 3 Results

#### 3.1 Spatial and temporal variations in the EAWM

The surface wind field in the East China Sea and the South China Sea adjacent to the mainland is mainly driven by land-sea pressure difference. Therefore, the surface wind field in this region can reflect the essential characteristics of the monsoon, namely land-sea heat contrast, and can more directly represent the variation of EAWM intensity (Chen et al. 2000). To reveal the spatial pattern of the EAWM, an EOF analysis for winter with a 10 m surface wind field during 1962–2020 is shown in Fig. 1a. The first EOF mode (EOF1) accounts for approximately 34.26% of the total variance and is effectively separated from the second EOF mode (23.26%) according to North (1982). As shown in Fig. 1a, EOF1 reflects a pattern of dominant strengthening (weakening) of the wintertime northerlies over East Asia and the adjacent ocean areas. The high consistency of the time series of EOF1 (PC1) and the EAWM index is shown in Fig. 1b. Their correlation coefficient is 0.88, far beyond the 99.9% confidence level, indicating that the EAWM index can also better reflect the circulation characteristics of the EAWM advancing from north to south and its variation characteristics with time, which is consistent with the previous analysis results (Chen et al. 2000). Moreover, the change of wind field is directly driven by change of pressure gradient that may intimately links with large-scale AM redistribution and potentially associated with the unbalance of inter-hemispheric AM or IHO. Therefore, in order to study the

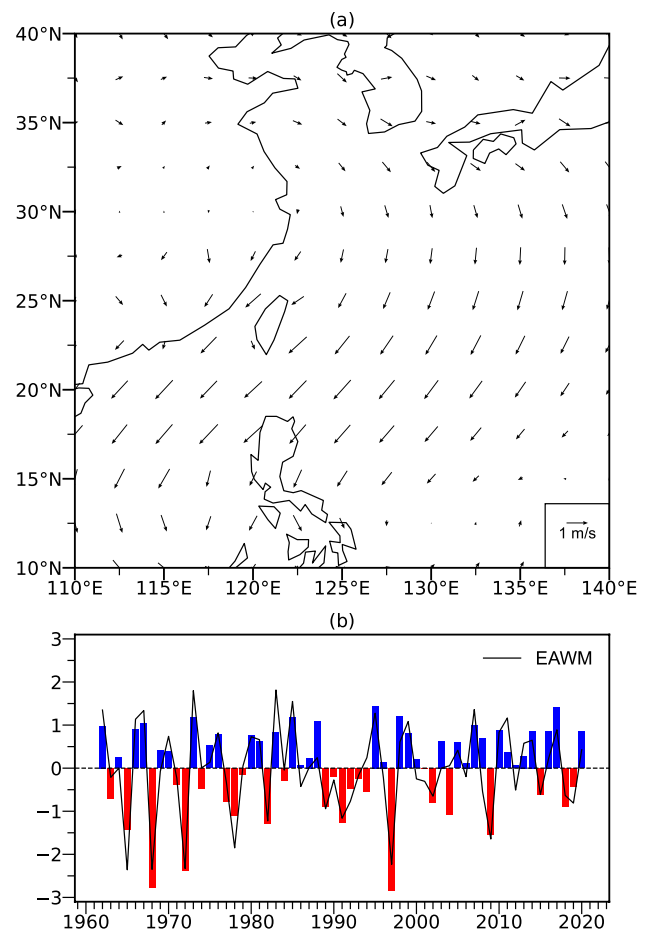
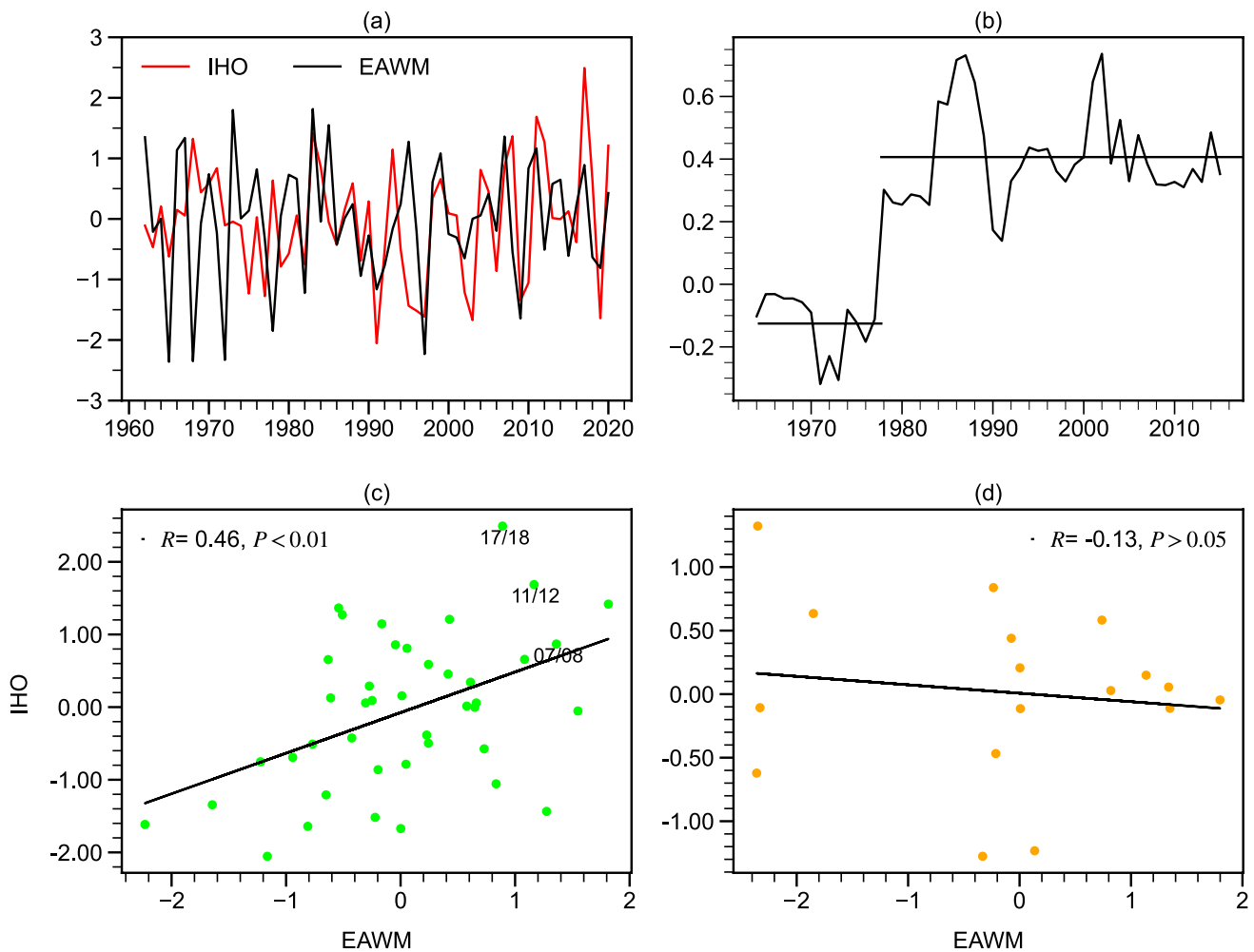


Fig. 1 First mode of EOF decomposition of 10 m anomalous winds in winter during 1962–2020 (a, unit: m/s), and its corresponding time series (bar) and monsoon index (solid line) (b)

relationship between IHO and monsoon, this surface-wind-based monsoon index is adopted in the following.

#### 3.2 Interdecadal changes in the relationship between the IHO and EAWM

Since the land-sea pressure difference is the main driving factor of the EAWM (Zeng and Li 2002), the EAWM is intimately related to the changes in semipermanent pressure systems, such as the Siberian High and Aleutian Low. This involves redistribution of AM over large scales such as the NH and even between the NH and SH (Carrera et al. 2003; Lu et al. 2008). As shown in Fig. 2a, there is a significant positive correlation between the detrended IHO and the EAWM index ( $r=0.25$ , above the 95% confidence level). More importantly, in the past decade, such as 2007/2008, 2011/2012 and 2017/2018, when large-scale persistent extreme low-temperature events occurred, the IHO index also had an extreme positive phase during the winter, consistent with the EAWM. Moreover, we found that the



**Fig. 2** Time series of detrended  $I_{\text{IHO}}$  and  $I_{\text{EAWM}}$  (a) and their 11-year running correlation (b, the black horizontal line shows their average over the two periods). Scatter plot of  $I_{\text{IHO}}$  and  $I_{\text{EAWM}}$  during 1962–

1978 (c) and 1979–2020 (d). Straight lines indicates the linear fitted lines. The mark below the dot represents the winter of the corresponding year

interannual variation of IHO and EAWM is more consistent in recent decades than the previous stage (Fig. 2a). This inspired us to explore a possible interdecadal change in the connection between the EAWM and IHO. We calculated the 11-year running correlation coefficient between the IHO and EAWM (Fig. 2b). In particular, IHO showed a weak negative correlation with the EAWM from 1962 to 1978, while they became a close positive correlation after 1979, indicating that the association between IHO and the EAWM has been significantly strengthened since 1979. Specifically, from 1979 to 2020 (Fig. 2c), there was a highly linear relationship, and the correlation coefficient between the two indices was as high as 0.47, exceeding the 95% confidence level. In contrast, the correlation between IHO and the EAWM index was weak ( $r = -0.13$ ) during 1962–1978 (Fig. 2d), and most of the IHO and EAWM index pairs also deviated from the linear fitting line, indicating their weak linear relation.

It should be pointed out that although satellite data were widely supplemented into global atmospheric reanalysis after 1979, the description of global atmospheric circulation before and after the satellite era could be affected to some extent. However, accelerated global warming since the late 1970s and its associated abrupt changes in global oceanic and atmospheric systems have been consistent, as revealed by multisource observation data. Moreover, the above changes were mainly exhibited in the middle and high latitudes, especially in the polar regions (Yanjuan and Xiuqun 2002). Under the background of global warming, the warming over the East Asian continent was significantly larger than that over the western Pacific Ocean, leading to a decrease in land-sea thermal differences and a weakening of the EAWM (Wang et al. 2001; He 2013). Therefore, this further suggests that the abrupt change of atmospheric system in the late 1970s may played an important role in regulating the interdecadal variation of

EAWM, and inspires us to further explore the cause of the decadal variation of the relationship between IHO and EAWM from the perspective of the global atmospheric system.

The redistribution of AM is directly linked to changes in regional surface pressure (SAP) as well as surface wind and thus plays a physically driven role in the low-level atmospheric circulation (van den Dool and Saha 1993). According to the correlation of the EAWM index with SAP from 1962 to 2020 (Fig. 3a), the Eurasian continental region is dominated by a large area of high positive correlation, while the negative correlation area is widely spread over the tropical and subtropical oceans and continental regions of 50°W–180, especially in the northwestern Pacific. This further indicates that the pressure gradient force caused by the thermal difference between land and sea is the direct driving factor of the EAWM. Notably, the area where the EAWM index is significantly related to the SAP is not limited to the East Asian continent and its adjacent oceans but also includes the East Pacific, North Atlantic and mid- and high latitudes of the SH. These globally broad significant correlations between the EAWM index and SAP suggest that the change in the EAWM may be linked to global AM redistribution and interhemispheric interactions. Further analysis of the correlation field between the IHO index and SAP from 1979 to 2020 (Fig. 3b) also shows a similar spatial distribution of correlations as in Fig. 3a. During 1979–2020, the abnormal distribution of the correlation coefficient of IHO with SAP in the north due to the south negative hemisphere reflected the out-of-phase correlation between the two hemispheres' AM and its association with the redistribution of AM and monsoon changes in East Asia. That is, there were larger positive (negative) significant areas in the Northern (Southern) Hemisphere. In contrast, the high-positive correlation area between IHO and SAP was widely distributed in the high latitudes of the NH and SH, while a large negative correlation area appeared in the middle and low latitudes during 1962–1978 (Fig. 3c). Specifically, when the IHO index was in positive phase, the AM in East Asia was abnormally lost, which was not conducive to the accumulation of cold air there. Meanwhile, there was abnormal mass accumulation in the midlatitude Pacific region, which weakened the pressure gradient force in the east–west direction, which was not conducive to the southwards invasion of cold air. In addition, the southern maritime continental area was occupied by an insignificant negative correlation area, which also led to the weakening of the north–south sea-land pressure gradient force and weakening of the EAWM.

To analyse the possible reasons for the interdecadal change in the relationship between the EAWM and IHO among the above two periods, the lower atmospheric circulation anomaly related to IHO was analysed by regression of surface wind on the IHO index. As shown in Fig. 4a,

the surface northerly wind in the northwestern Pacific was strengthened when the IHO was in the positive phase during 1979–2020. Meanwhile, the eastern coast of China and southern Japan north of 30° N were accompanied by significant northerly anomalies. The EAWM was therefore intensified as the IHO index value increased. This corresponds well to significant increases in the westwards pressure gradients around East Asia in Fig. 3b. However, the influence of the IHO on the lower atmospheric circulation during 1962–1978 was pronouncedly weaker than that during 1979–2020. The lower troposphere of East Asia was occupied by abnormal cyclonic circulation in positive IHO years, bringing southerly anomalies in the midlatitude monsoon region (Fig. 4b). In addition, the correlation between the wind field and IHO in the low latitudes of the EAWM region was neutral.

To further show the driving role of the IHO on the sea-land pressure gradient and winter monsoon in East Asia, we constructed a sea-land pressure change index (PI) to highlight the key regions associated with both the EAWM and IHO. Since the land-sea pressure difference is the main driver of EAWM, the significant correlated areas between EAWM and SAP display almost the entire Eurasian continent and its adjacent seas in Fig. 3a. However, considering the driven physical role of the Siberian High (Miao and wang 2020), the Maritime Continent low (Wang and Chen 2014a, b) as well as the SAP in North China, we define the PI based on the regional mean pressure over the above three regions, and the expression of the PI is as follows:

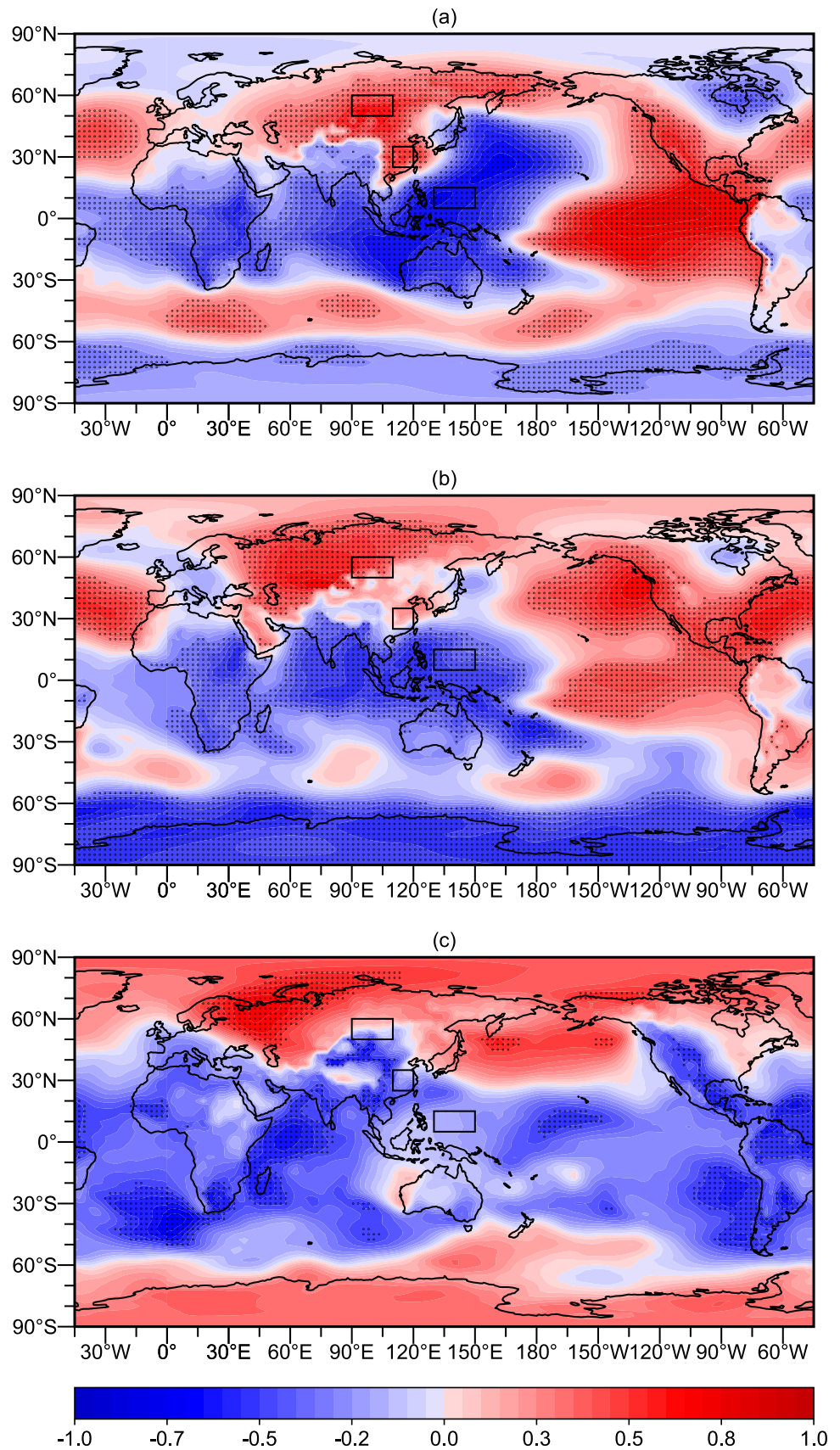
$$PI = \frac{1}{2}A_1^* + \frac{1}{2}A_2^* - A_3^* \quad (2)$$

where  $A_1^*$ ,  $A_2^*$  and  $A_3^*$  indicate the standardization area-average SAP over Siberia (50°–60° N, 90°–110° E), North China (25°–35° N, 110°–120° E) and the maritime continent (5°–15° N, 130°–150° E), respectively.

The correlation coefficient between the PI and the EAWM index reached 0.88 above the 99% *t* test confidence level, indicating that the PI represents the variability in the intensity of the EAWM well and suggesting that land-sea pressure differences, especially among these three key areas, play an important role in the variation in the EAWM.

Furthermore, the correlation coefficients between the IHO and PI in the two periods were calculated (Fig. 5). Comparing the two periods, it is not difficult to find that the relationship between the IHO and land-sea pressure difference from 1979 to 2020 was significantly closer than that of the previous period ( $r=0.58$ , exceeding the 99% confidence level), suggesting that there was a significant positive correlation between the IHO and EAWM in this period (Fig. 5a). Meanwhile, as the values of  $I_{IHO}$  and PI increased, the winter-mean SAT in the eastern part of China generally obviously decreased. Furthermore, the regional cold wave intensity (Zhang et al. 2018) in East

**Fig. 3** Correlation fields between EAWM and SAP (a, 1962–2020), IHO and SAP (b, 1979–2020) and (c, 1962–1978), dotted areas indicate the 99% confidence levels based on  $t$ -test. The three rectangles indicate the areas used to define the PI index



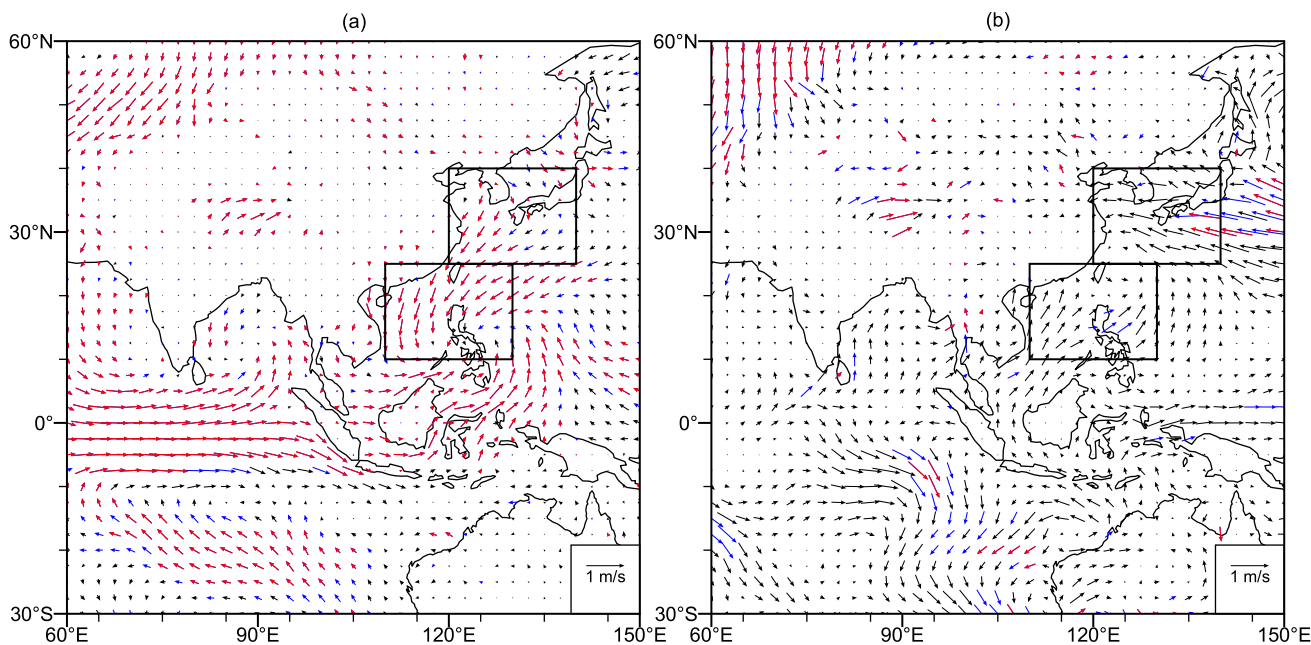


**Fig. 4** Regression of surface wind field (arrows, units:m/s) on IHO **(a)**, 1979–2020) and **(b)**, 1962–1978). Blue and red arrows indicate the 95% and 99% confidence levels based on F-test, and the black rectangular box indicates the monsoon area

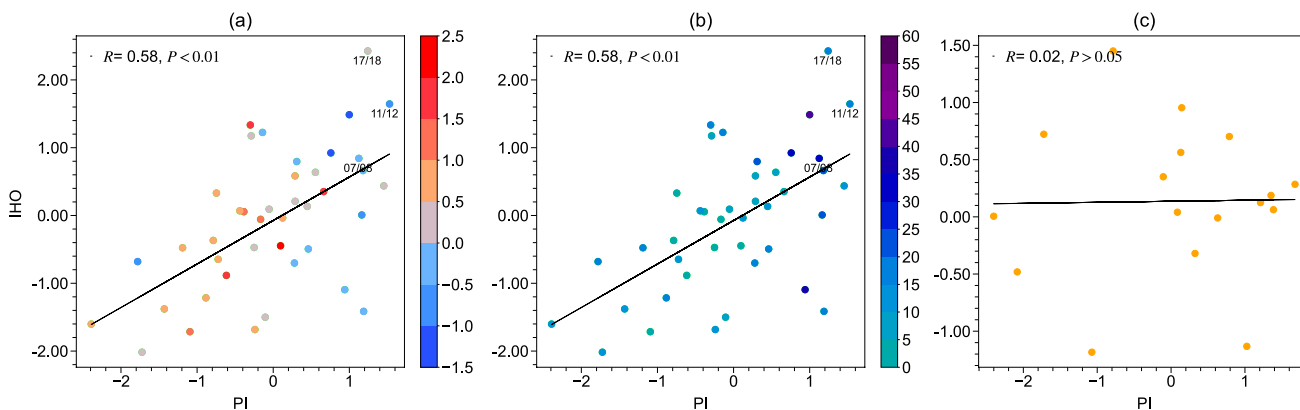


**Fig. 5** Scatter correlation between detrended PI index and  $I_{IHO}$  from 1979 to 2020 **(a, b)** and 1962–1978 **(c)**. Colors indicate average winter temperature **(a)**, unit: °C) and cold wave intensity **(b)**, unit: day)

over East China (22.5°–42.5° N, 102.5°–122.5° E).The mark below the dot represents the winter of the corresponding year. Straight lines indicates the linear fitted lines

China in the past ten years has mostly been concentrated in strong IHO and EAWM years (Fig. 5b). For example, in 2007/2008, 2011/2012, 2017/2018 and during other regional persistent extreme low-temperature events, the values of the PI and IHO index were both large. Here, the cold wave intensity was expressed by two consecutive days or more when the daily SAT was lower than the area-averaged SAT in winter from 1962 to 2020 by at least one standard deviation, and the standard deviation ( $\sigma$ ) used was the average of the surface temperature daily standard deviation in winter (December 1st to February 28th). In contrast, the relationship between IHO and the

sea-land pressure difference was weak from 1962 to 1978, which also indicates that there was not a weak correlation between IHO and the EAWM (Fig. 5c).

The correlation coefficients between the IHO index and SAT clearly show that SAT over most parts of China (except the Qinghai–Tibet Plateau) decreased significantly as the IHO index increased from 1979 to 2019 (Fig. 6a). In particular, when the IHO index increased by one standard deviation, the area-averaged temperature in East China decreased by 0.21 degrees, and the cold wave intensity increased by 2.61 days. This further indicates the intimate correlation between IHO and winter temperature in China

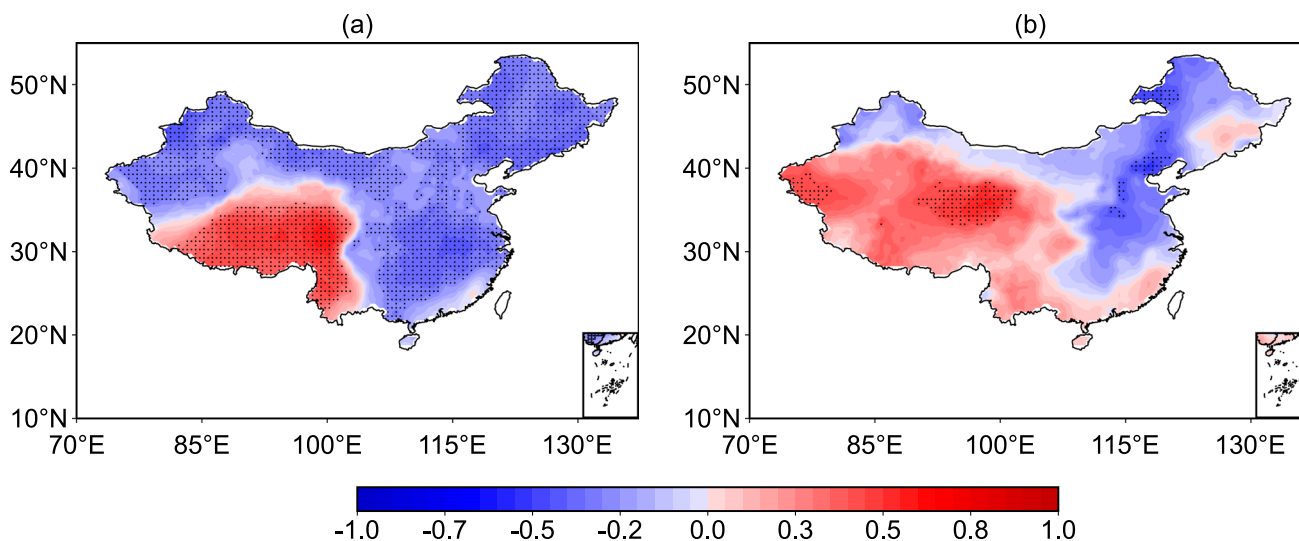


**Fig. 6** Correlation fields between IHO(detrended) and winter SAT in China from CN05.1 during 1979–2019 (a) and 1962–1978 (b), with dotted areas indicating the 90% confidence levels based on *t*-test

during 1979–2019. However, the relationship between IHO and winter-mean SAT in China from 1962 to 1978 was not close to that during 1979–2019 and only showed limited significant correlation areas in the northern part of China (Fig. 6b).

#### 4 Possible mechanisms

To reveal a possible formation mechanism of the interdecadal variation in the relationship between the IHO and EAWM, this section discusses the features and driving factors of the changes in the IHO-associated imbalance and redistribution of AM between the two hemispheres. According to the composite difference map of SAP in the two periods (Fig. 7a), the SAP anomalies in the high latitude areas of the two hemispheres, especially for the Antarctic regions, clearly exhibited significant reduction characteristics during 1979–2020 compared with the previous period. As shown in Table 1, further calculation also shows that the AM in Antarctica during 1979–2020 has changed more significantly than that in Arctic during the previous period. Therefore, AM deficit over Antarctica is the main influence factor that leads to the exacerbation of AM imbalance between the two hemispheres after 1979. Because the SAP is proportional to the mass of the air column and the global conservation of AM, the AM defect in Antarctica indicates that the AM of other areas was abnormally accumulated. Correspondingly, the SAP in the middle and low latitudes obviously increased, including on the African continent, East Asia, and the equatorial Middle East Pacific region. In particular, the SAP in East Asia increased significantly, leading to an

increase in the air pressure difference between land and sea and a strengthening of the relationship between the IHO and EAWM during 1979–2020.

To quantitatively highlight the driving role of the deficit of AM over Antarctica on the decrease in AM in the SH and an increase in the interhemispheric imbalance of AM. The AM in the Antarctic region ( $m_{AP}$ ) and the contribution of  $m_{AP}$  to the  $I_{IHO}$  ( $C$ ) are expressed by Formula (3).

$$\left. \begin{aligned} m_{AP} &= \frac{2\pi a^2 f_D}{g_0} \int_{-\frac{\pi}{2}}^{\frac{\pi}{3}} \overline{P_s}(\varphi) \cos \varphi d\varphi \\ C &= \frac{m_{AP}}{m_{NH} - m_{SH}} \end{aligned} \right\} \quad (3)$$

A significant downwards trend of  $m_{AP}$  during the last 60 years ( $-0.021 \times 10^{15}$  kg/10 yr, above the 99% confidence level) is clearly shown in Fig. 7b. The pronounced decreasing trend resulted in a dramatic difference between 1962–1978 and 1979–2020. The composite of  $m_{AP}$  decreased significantly by  $0.057 \times 10^{15}$  kg during 1979–2020 compared with that during 1962–1978 (passing the 99% confidence level *t* test). Furthermore, the contribution rate of AM changes to IHO in Antarctica also shows an obvious linear growth trend, and there was an obvious interdecadal enhancement from 1979 to 2020. As documented in Table 1, the  $m_{AP}$  deficit directly corresponds to a decrease of  $0.14 \times 10^{15}$  kg for the AM in the SH during 1979–2020 compared to the previous period. In contrast, the AM in the NH abnormally accumulated  $0.62 \times 10^{15}$  kg. Although the AM in the SH was higher than that in the NH due to the wider ocean surface distribution in winter, the composite difference in AM between



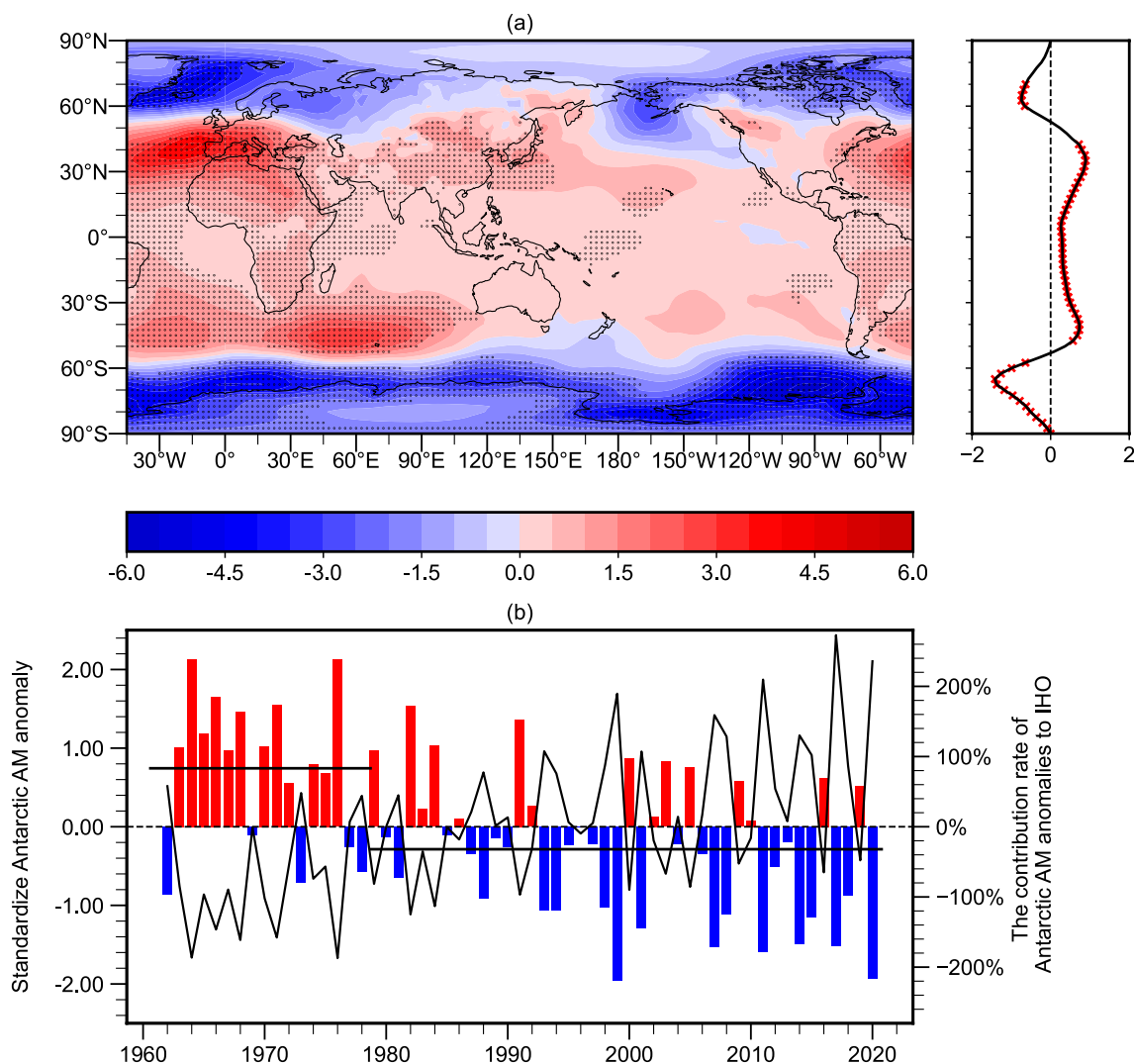


**Fig. 7** Composite difference in the SAP between 1962–1978 and 1979–2020 (a, the latter period minus the previous period, unit: hPa). The solid line in the right graph shows the zonal average of the difference in SAP on the left side multiplied by the cosine of the corresponding latitudes (area weight coefficient). Dotted areas and red

marks indicate the 95% confidence levels based on a two-sided Student’s *t* test. The standardized Antarctic AM (b, histogram, black horizontal line indicates its average in the two periods) and the contribution rate of Antarctic mass change to IHO (b, solid line)

**Table 1** The combined deviation of the two hemispheres’ mass (unit:  $\times 10^{15}$  kg) and area-weighted average SAP (hPa) in 1962–1978 and 1979–2020

	NH		SH		Arctic		Antarctic		NH–SH	
	AM	SAP	AM	SAP	AM	SAP	AM	SAP	AM	SAP
1962–1978	-0.44	-0.17	0.096	0.04	0.41	0.16	0.75	0.29	-0.54	-0.21
1979–2020	0.18	0.07	-0.039	-0.01	-0.16	-0.06	-0.30	-0.12	0.22	0.08
Later period-previous period	<b>0.62*</b>	<b>0.24*</b>	-0.14	-0.05	-0.57	-0.22	<b>-1.058*</b>	<b>-0.40*</b>	<b>0.75*</b>	<b>0.29*</b>

Correlation coefficients in bold are significant at the 99% confidence level. Correlation coefficients marked with an asterisk are significant at the 95% confidence level

the NH and SH had notably positive anomalies between the above two periods, with a value of  $0.75 \times 10^{15}$  kg. Consequently, the reduction in  $m_{AP}$  induced an obvious decrease in the AM in the SH and a significant increase in the AM difference between the NH and SH.

The contrasts in the meridional and vertical distributions of air temperature and geopotential height anomalies before and after 1979 are shown in Fig. 8a and b. Conspicuous cooling occurred in the high latitudes of the SH during 1979–2020, accompanied by a strengthened polar vortex and a columnar lower geopotential that was consistent with the pronounced reduction in Antarctic AM. Meanwhile, most areas outside Antarctica exhibited notable warming events and positive geopotential heights in concert with the increase in AM in these areas. In contrast, the temperature and geopotential height had a nearly opposite pattern during 1962–1978 (Fig. 8b). By comparing the meridional changes in the vertical temperature profile between the two periods, the dramatic turning of the thermal structure in the SH high-latitude area corresponds well to the strengthening of the IHO after 1979. This turning could relate to global warming and its uneven spatial distribution (Jones 1999, Johanson 2007). In addition, the regression analysis of IHO vertical profile, temperature and geopotential height before and after 1979 is shown in Fig. 8c and d. During 1979–2020, when the IHO was strong, significant negative air temperature anomalies appeared over the Antarctic, the geopotential height and AM decreased. However, during 1962–1978, there was no significant relationship between air temperature, geopotential height and IHO. This suggests that the loss of AM caused by the abnormal cooling over Antarctica after 1979 was the direct cause of the enhanced IHO.

To further analysis the causality of in numerical simulation, we used the MPI-ESM1-2-HR model in CMIP6 to verify the role of Antarctic AM in driving the interhemispheric change. The regression field distribution of IHO and SAP in Fig. 9a is consistent with the results obtained above. During 1979–2020, when the IHO was stronger, the SAP in Antarctica decreased significantly, and the sea-land pressure difference in East Asia increased significantly. Further calculation shows that the correlation coefficient between IHO and PI index in the model is as high as 0.50 (above 99% confidence level), indicating a close relationship between IHO and EAWM after 1979. In addition, obvious negative temperature anomalies appear in the Antarctic region and the geopotential height decreases as IHO index increase (Fig. 9b), which also demonstrates that the decrease of AM in the Antarctic plays a driving role in the imbalance between NH and SH.

It is worth noting that the key area causing the abrupt change in the connection between the IHO and EAWM was located in the high-latitude area of the SH, and the atmospheric thermal situation in this area had also changed

obviously in the two periods. In both periods, the large values of temperature anomalies were near the upper troposphere/lower stratosphere (UTLS). Consistently, as shown by NOAA/STAR observational temperature (Wang and Zou 2014), atmospheric warming also occurred in the upper troposphere in tropical areas with a 0.12 K/10 yr upwards trend, accompanied by a significant decreasing trend in the Antarctic region (0.048 K/10 yr) (Fig. S2). Since the change in ozone plays a driving role in the variation in temperature in the UTLS by radiative effects (Fomichev 2009, Hartmann 2000), we also calculated the scattered distribution of ozone and temperature at the 150–100 hPa level in Antarctica to explore the driving factors for the interdecadal change in IHO. There was a significant positive correlation between ozone and temperature (Fig. 10a), and the correlation coefficient was 0.86 (exceeding the 99% confidence level). Additionally, the significant positive correlation between ozone and temperature was also shown in OSIRIS observational ozone and RAOBCORE/RICH satellite temperature datasets during 2014–2016 (Fig. 10b), with a correlation coefficient of 0.94. More importantly, the 150–100 hPa mean Antarctic ozone mass during 1979–2016 was significantly reduced by  $5.22 \times 10^9$  kg compared to that during 1962–1978. The decrease in ozone content resulted in significant cooling in the UTLS with a composite difference of  $-1.92$  K.

Interestingly, a seesaw pattern of ozone and temperature in UTLS occurred between low latitudes and mid-high latitudes in the SH, as shown in Fig. 9, which is similar to the results of Randel et al. (2002) and Yulaeva et al. (1994). The Brewer-Dobson circulation driven by planetary wave convergence carries ozone from high concentrations generated over the equator to the poles, resulting in increased ozone at high latitudes and decreased ozone at low latitudes (Chen et al. 1992). According to Wang et al. (2021), the obvious warming of the lower stratosphere in the tropical region leads to the increase of the meridian temperature gradient in the SH, which makes the stratosphere latitudinal phase stronger, and the distance between the interface ( $U=0$ ) and the wave reflector larger. More planetary waves in the upper stratosphere are reflected and diverged. This weakens the ozone transport to the polar region related to the residual circulation and reduces ozone content in the Antarctic region, thus forming the anti-phase change of the low stratosphere temperature in the Antarctic and tropical regions. Therefore, under the background of global warming (especially in the tropical UTLS), the ozone and temperature in the Antarctic decreased significantly, resulting in the AM defect in the Antarctic, accompanied by the accumulation of AM in the NH, especially in the Eastern Hemisphere.

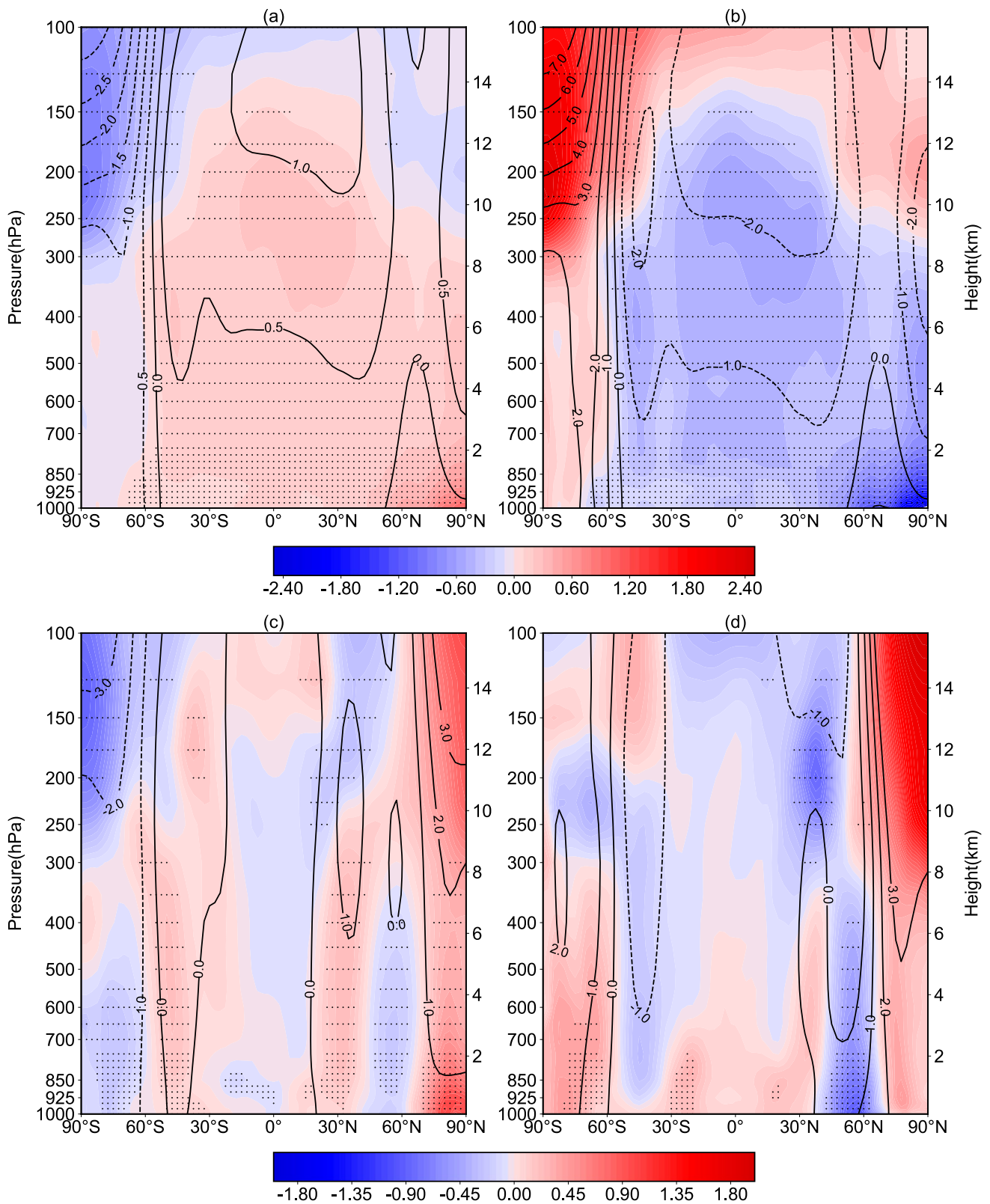


**Fig. 8** The zonal mean combined deviations of temperature (shadow, unit:K) and geopotential height (solid line, unit: dgm) for 1979–2020 (a) and 1962–1978 (b) are distributed vertically in the warp direction. The dotted area represent the 95% confidence levels based on the two-sided Student's *t* test, respectively. Zonal mean regression analysis

of air temperature (shadow, unit:K) and geopotential height (solid line, unit:dgm) for 1979–2020 (c) and 1962–1978 (d) are distributed vertically in the warp direction. The dotted area represent 90% confidence levels based on the F test, respectively

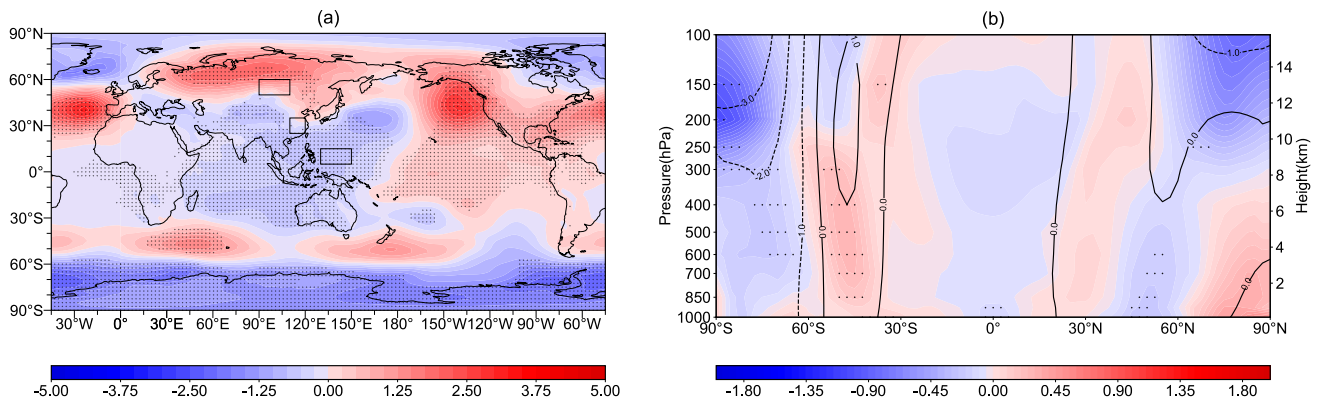


**Fig. 9** The zonal mean regression analysis of surface pressure (**a**, unit:hPa), air temperature (**b**, shadow, unit: K) and geopotential height (**b**, solid line, unit: dgm) during 1979–2013 are distributed

vertically in the warp direction from CMIP6. The dotted area represent the 90% confidence level based on the F test. The three rectangles indicate the areas used to define the PI index

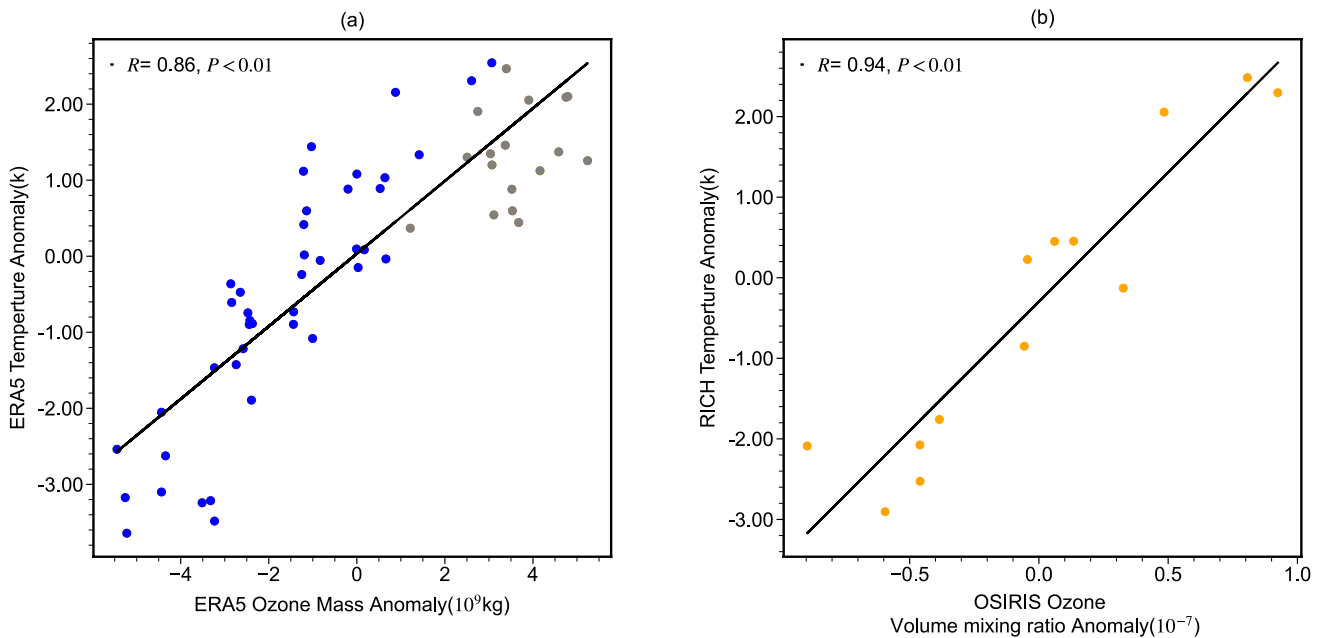


**Fig. 10** Scatter plot of atmospheric mean temperature (unit: K) and ozone mass anomaly (unit:  $10^9$  kg) from ERA5 during 1962 to 1978 (gray, **a**) and 1979 to 2020 (blue, **a**), atmospheric mean temperature

(from RICH, unit: K) and ozone Volume mixing ratio anomaly (from OSIRIS, unit:  $10^{-7}$ ) at 150–100 hPa in Antarctica (60–90° S) in winter, Straight lines indicates the linear fitted lines

## 5 Summary and discussion

In this paper, the interdecadal variation in the relationship between the IHO and EAWM in winter and its influence on the winter climate in China are analysed, and the possible formation mechanisms of IHO enhancement in winter since 1979 are further discussed. The conclusions are as follows:

1. An obvious multidecadal intensification of the correlation between the EAWM and IHO occurred during the past four decades. In particular, the relationship

between IHO and the EAWM was neutral before 1979. In contrast, a significant positive correlation ( $r=0.46$ ) between the two occurred in the last 40 years, which was associated with notable accumulation (loss) of AM in East Asia (maritime continental areas). Such large-scale changes in AM intensified the land-sea pressure contrast in East Asia and enhanced the EAWM. As a result, the IHO-associated intensified interhemispheric AM imbalance favoured severe winters in eastern China.

2. The AM in SH has lost  $0.14 \times 10^{15}$  kg in the last 40 years, compared to the period of 1962–1979, and the Antarctic region is the key area of net AM exportation, with a loss

of  $1.06 \times 10^{15}$  kg. Due to the global conservation of dry air mass, the AM in the NH increased significantly by  $0.62 \times 10^{15}$  kg compared with the previous period. The main AM build-up areas involved were on the African continent, East Asia and the equatorial Middle East Pacific region. Correspondingly, the land-sea pressure gradient in East Asia notably increased, leading to an interdecadal enhancement of the connection between the IHO and EAWM.

3. The global tropospheric atmosphere has been significantly warming since 1979, especially in the tropical UTLS. A seesaw teleconnection has emerged between the tropics and upper troposphere temperature and ozone in the Antarctic. Correspondingly, Antarctic ozone has been pronouncedly depleted in association with warming in the tropical UTLS, leading to abnormal columnar cooling in the high latitudes of the SH. The Antarctic polar vortex has intensified and AM in the Antarctic and SH (NH) has decreased (increased) as a result, which has given rise to the interdecadal enhancement of IHO.

It is worth noting that the research in this paper reveals that Antarctic ozone depletion and associated radiative cooling have resulted in the loss of AM in the high latitudes of the SH over the past four decades. However, distinct from the relationship between the change in AM and temperature in the Antarctic, there has been a warming amplification effect in the Arctic, and the temperature of the air column in the Arctic has risen in contrast. Previous studies have shown that driving factors, such as radiation feedback of decreasing sea ice (Larsen et al. 2014) and enhanced transmission of AMOC to extreme heat (Deng 2022), could play important roles in amplified Arctic warming. Therefore, although the SAP also decreased obviously in the Arctic, the air column and geopotential high have shown obvious lifting features.

In addition, with the implementation of the Montreal Protocol, the concentration of ozone-depleting substances in the atmosphere has been effectively controlled, and global ozone has recovered. However, ozone in the upper troposphere of Antarctica is still decreasing (Kumar 2021). It has been pointed out that the warming of the tropical regions strengthens the westerlies in the midlatitudes of the SH due to the increase in the meridional temperature gradient, leading to a reduction in atmospheric heat transfer into the Antarctic. Associated cooling in the Antarctic provides the necessary low-temperature conditions for the decomposition and reduction of Antarctic ozone (Wang 2015). In addition, the strengthened westerlies also hinder AM transport into the Antarctic, which will further lead to ozone loss. Among them, the change in residual circulation could be an important driving factor affecting the ozone distribution in the UTLS. The dynamic mechanisms

of ozone loss in the Antarctic advection lower layer still need to be further explored through numerical simulation.

**Supplementary Information** The online version contains supplementary material available at <https://doi.org/10.1007/s00382-023-06810-x>.

**Author contributions** CL and LZ wrote the main manuscript text. LZ and NQ prepare Figs. 1–10. ZG provide discussions and advices for the improvement of the manuscript. All authors reviewed the manuscript.

**Funding** This work was supported jointly by the National Natural Science Foundation of China (Grant No. 41975073), the National Key Research and Development Program of China (Grant No. 2019YFC1510201), Shanghai Science Committee (20dz1200401) and Wuxi University Research Start-up Fund for Introduced Talents.

**Data availability statement** ERA5 reanalysis products were download from the European Centre for Medium-Range Weather Forecasts (ECMWF) at <https://doi.org/10.24381/cds.adbb2d47>. The gridded dataset (CN05.1) were obtained from <https://ccrc.iap.ac.cn/resource/detail?id=228>. The monthly zonal average data of ozone detected by the OSIRIS satellite of the SPARC data plan download from <https://doi.org/10.5281/zenodo.4265393>. RAOBCORE/RICH temperature were download from <https://srvx1.img.univie.ac.at/webdata/haimberger/v1.5.1>.

## Declarations

**Conflict of interest** The authors have no relevant financial or non-financial interests to disclose.

## References

- Carrera ML, Gyakum JR (2003) Significant events of interhemispheric atmospheric mass exchange: composite structure and evolution. *J Clim* 16(24):4061–4078. [https://doi.org/10.1175/1520-0442\(2003\)016%3c4061:SEOIAM%3e2.0.CO;2](https://doi.org/10.1175/1520-0442(2003)016%3c4061:SEOIAM%3e2.0.CO;2)
- Chen P, Robinson W (1992) Propagation of planetary waves between the troposphere and stratosphere. *J Atmos Sci* 49(24):2533–2545. [https://doi.org/10.1175/1520-0469\(1992\)049%3c2533:POP-WBT%3e2.0.CO;2](https://doi.org/10.1175/1520-0469(1992)049%3c2533:POP-WBT%3e2.0.CO;2)
- Chen W, Graf HF, Huang R (2000) The interannual variability of east Asian winter monsoon and its relation to the summer monsoon. *Adv Atmos Sci* 17(1):48–60. <https://doi.org/10.1007/s00376-000-0042-5>
- Chen W, Yang S, Huang R (2005) Relationship between stationary planetary wave activity and the East Asian winter monsoon. *J Geophys Res*. <https://doi.org/10.1029/2004JD005669>
- Chen Z, Wu R, Chen W (2014) Distinguishing interannual variations of the northern and southern modes of the East Asian winter monsoon. *J Clim* 27(2):835–851. <https://doi.org/10.1175/JCLI-D-13-00314.1>
- Chen Z, Wu R, Wang Z (2019a) Impacts of summer north Atlantic sea surface temperature anomalies on the east Asian winter monsoon variability. *J Clim* 32(19), 6513–6532. <https://journals.ametsoc.org/view/journals/clim/32/19/jcli-d-19-0061.1.xml>
- Chen W, Wang L, Feng J, Wen Z, Ma T, Yang X, Wang C (2019b) Recent progress in studies of the variabilities and mechanisms of the East Asian monsoon in a changing climate. *Adv Atmos Sci* 36:887–901. <https://doi.org/10.1007/s00376-019-8230-y>

- Deng J, Dai A (2022) Sea ice–air interactions amplify multidecadal variability in the North Atlantic and Arctic region. *Nat Commun* 13:2100. <https://doi.org/10.1038/s41467-022-29810-7>
- Ding Y, Liu Y, Liang S, Ma X, Zhang Y, Si D, Liang P, Song Y, Zhang J (2014) Interdecadal variability of the East Asian winter monsoon and its possible links to global climate change. *J Meteorol Res* 28:693–713. <https://doi.org/10.1007/s13351-014-4046-y>
- Fomichev V (2009) The radiative energy budget of the middle atmosphere and its parameterization in general circulation models. *J Atmos Solar Terr Phys* 71:1577–1585. <https://doi.org/10.1016/J.JASTP.2009.04.007>
- Gao XJ (2013) A gridded daily observation dataset over China region and comparison with the other datasets. *Chin J Geophys* 56(4):1102–1111. <https://doi.org/10.6038/g20130406>
- Gong H, Wang L, Chen W, Wu R (2019) Attribution of the East Asian winter temperature trends during 1979–2018: role of external forcing and internal variability. *Geophys Res Lett* 46:10874–10881. <https://doi.org/10.1029/2019GL084154>
- Guan Z, Yamagata T (2001) Interhemispheric oscillations in the surface air pressure field. *Geophys Res Lett* 28:263–266. <https://doi.org/10.1029/2000GL011563>
- Haimberger L, Tavolato C, Sperka S (2012) Homogenization of the global radiosonde temperature dataset through combined comparison with reanalysis background series and neighboring stations. *J Clim* 25(23):8108–8131. <https://doi.org/10.1175/JCLI-D-11-00668.1>
- Hartmann DL, Wallace JM, Limpasuvan V et al (2000) Can ozone depletion and global warming interact to produce rapid climate change. *Proc Natl Acad Sci* 97(4):1412–1417. <https://doi.org/10.1073/PNAS.97.4.1412>
- He S (2013) Reduction of the East Asian winter monsoon interannual variability after the mid-1980s and possible cause. *Chin Sci Bull* 58:1331–1338. <https://doi.org/10.1007/s11434-012-5468-5>
- He JH, Ju JH, Wen ZP, Lu JM, Jin QH (2007) A review of recent advances in research on Asian monsoon in China. *Adv Atmos Sci* 24:972–992. <https://doi.org/10.1007/s00376-007-0972-2>
- Hegglin MI, Tegtmeier S, Anderson J et al (2020) SPARC Data Initiative monthly zonal mean composition measurements from stratospheric limb sounders (1978–2018). Zenodo. <https://doi.org/10.5281/zenodo.4265393>
- Hu C, Yang S, Wu Q (2015) An optimal index for measuring the effect of East Asian winter monsoon on China winter temperature. *Clim Dyn* 45:2571–2589. <https://doi.org/10.1007/s00382-015-2493-5>
- Jeong J, Ou T, Linderholm HW, Kim BM, Kim SJ, Kug JS, Chen D (2011) Recent recovery of the Siberian high intensity. *J Geophys Res* 116:D23102. <https://doi.org/10.1029/2011JD015904>
- Johanson CM, Fu Q (2007) Antarctic atmospheric temperature trend patterns from satellite observations. *Geophys Res Lett* 34:L12703. <https://doi.org/10.1029/2006GL029108>
- Jones PD, New M, Parker DE et al (1999) Surface air temperature and its changes over the past 150 years. *Rev Geophys* 37(2):173–199. <https://doi.org/10.1029/1999RG900002>
- Kumar P, Kuttippura J, von der Gathen P et al (2021) The increasing surface ozone and tropospheric ozone in Antarctica and their possible drivers. *Environ Sci Technol* 55:8542–8553. <https://doi.org/10.1021/acs.est.0c08491>
- Larsen JN, Anisimov OA, Constable A et al (2014) Polar regions. In: Barros VR, Field CB, Dokken DJ et al (eds) *Climate change Impacts, adaptation, and vulnerability. Part B regional aspects*. Cambridge University Press, Cambridge, pp 1567–1612. <https://doi.org/10.1017/CBO9781107415386>
- Lim YK, Kim HD (2016) Comparison of the impact of the Arctic Oscillation and Eurasian teleconnection on interannual variation in East Asian winter temperatures and monsoon. *Theor Appl Climatol* 124:267–279. <https://doi.org/10.1007/s00704-015-1418-x>
- Lu C, Guan Z, Mei S, Qin Y (2008) The seasonal cycle of inter-hemispheric oscillations in mass field of the global atmosphere. *Chin Sci Bull* 53:3226–3234. <https://doi.org/10.1007/S11434-008-0316-3>
- Lu C, Guan Z, Yong-hua L, Ying-ying B (2013) Interdecadal linkages between the Pacific decadal oscillation and interhemispheric air mass oscillation and their possible connections with East Asian monsoon. *Chin J Geophys* 56:117–128. <https://doi.org/10.1002/cjg2.20012>
- Lu C, Xie S, Qin Y, Zhou J (2016) Recent intensified winter coldness in the mid-high latitudes of Eurasia and its relationship with daily extreme low temperature variability. *Adv Meteorol.* <https://doi.org/10.1155/2016/3679291>
- Luo X, Wang B (2019) How autumn Eurasian snow anomalies affect East Asian winter monsoon: a numerical study. *Clim Dyn* 52:69–82. <https://doi.org/10.1007/s00382-018-4138-y>
- Ma T, Chen W (2021) Climate variability of the East Asian winter monsoon and associated extratropical–tropical interaction: a review. *Ann NY Acad Sci* 1504:44–62. <https://doi.org/10.1111/nyas.14620>
- Miao J, Wang T (2020) Decadal variations of the East Asian winter monsoon in recent decades. *Atmos Sci Lett.* <https://doi.org/10.1002/asl.960>
- Miao J, Wang T, Wang H, Zhu Y, Sun J (2018) Interdecadal weakening of the East Asian winter monsoon in the mid-1980s: the roles of external forcings. *J Clim* 31:8985–9000. <https://doi.org/10.1175/JCLI-D-17-0868.1>
- North GR, Bell TL, Cahalan RF et al (1982) Sampling errors in the estimation of Empirical Orthogonal Functions. *Mon Weather Rev* 110(7):699–706. [https://doi.org/10.1175/1520-0493\(1982\)110%3c0699:SEITEO%3e2.0.CO;2](https://doi.org/10.1175/1520-0493(1982)110%3c0699:SEITEO%3e2.0.CO;2)
- Randel WJ, Wu F, Stolarski R (2002) Changes in column ozone correlated with the stratospheric EP flux. *J Meteorol Soc Jpn* 80(4B):849–862. <https://doi.org/10.2151/jmsj.80.849>
- Song L, Wu R (2017) Processes for occurrence of strong cold events over Eastern China. *J Clim* 30:9247–9266. <https://doi.org/10.1175/JCLI-D-16-0857.1>
- Song L, Wu R (2019) Combined effects of the MJO and the Arctic Oscillation on the intraseasonal eastern China winter temperature variations. *J Clim* 32:2295–2311. <https://doi.org/10.1175/JCLI-D-18-0625.1>
- Sun B, Wang HJ, Zhou BT (2019) Climatic condition and synoptic regimes of two intense snowfall events in eastern China and implications for climate variability. *J Geophys Res Atmos* 124:926–941. <https://doi.org/10.1029/2018JD029921>
- Sung M, Lim G, Kug J (2010) Phase asymmetric downstream development of the North Atlantic Oscillation and its impact on the East Asian winter monsoon. *J Geophys Res* 115:156–156. <https://doi.org/10.1029/2009JD013153>
- van den Dool H, Saha S (1993) Seasonal redistribution and conservation of atmospheric mass in a general circulation model. *J Clim* 6:22–30. [https://doi.org/10.1175/1520-0442\(1993\)006%3c0022:SRACOA%3e2.0.CO;2](https://doi.org/10.1175/1520-0442(1993)006%3c0022:SRACOA%3e2.0.CO;2)
- Wang HJ (2001) The weakening of the Asian monsoon circulation after the end of 1970s. *Adv Atmos Sci* 18(3):376–386. <https://doi.org/10.1007/BF02919316>
- Wang L, Chen W (2014a) The East Asian winter monsoon: reamplification in the mid-2000s. *Chin Sci Bull* 59(4):430–436. <https://doi.org/10.1007/s11434-013-0029-0>
- Wang L, Chen W (2014b) An Intensity Index for the East Asian Winter Monsoon. *J Clim* 27(6):2361–2374. <https://doi.org/10.1175/JCLI-D-13-00086.1>
- Wang L, Huang R, Gu L, Chen W, Kang LH (2009) Interdecadal variations of the East Asian winter monsoon and their association with quasi-stationary planetary wave activity. *J Clim* 22:4860–4872. <https://doi.org/10.1175/2009JCLI2973.1>

- Wang Z, Zhang X, Guan Z et al (2015) An atmospheric origin of the multi-decadal bipolar seesaw. *Sci Rep* 5:8909. <https://doi.org/10.1038/srep08909>
- Wang Z, Zhang J, Wang T, Feng W, Hu Y, Xu X (2021) Analysis of the Antarctic Ozone Hole in November. *J Clim*, 34(16),6513–6529. <https://journals.ametsoc.org/view/journals/clim/34/16/JCLI-D-20-0906.1.xml>
- Wang WH, Zou CZ (2014) AMSU-A-Only atmospheric temperature data records from the lower troposphere to the top of the stratosphere. *J Atmos Oceanic Technol* 31:808–825. <https://doi.org/10.1175/JTECH-D-13-00134.1>
- Wu B, Su J, Zhang R (2011) Effects of autumn–winter arctic sea ice on winter Siberian high. *Chin Sci Bull* 56(30):3220–3228. <https://doi.org/10.1007/s11434-011-4696-4>
- Yang L, Wu B (2013) Interdecadal variations of the East Asian winter surface air temperature and possible causes. *Chin Sci Bull* 58:3969–3977. <https://doi.org/10.1007/s11434-013-5911-2>
- Yanjuan G, Xiuqun Y (2002) Temporal and spatial characteristics of interannual and interdecadal variations in the global ocean-atmosphere system. *Scientia Meteorologica Sinica* 22(2):127–137 (in Chinese)
- Yao S, Sun Q, Huang Q, Chu P (2016) The 10–30-day intraseasonal variation of the East Asian winter monsoon: the temperature mode. *Dyn Atmos Oceans* 75:91–101. <https://doi.org/10.1016/j.dynatmoce.2016.07.001>
- You J, Jian M, Gao S, Cai J (2021) Interdecadal change of the winter–spring tropospheric temperature over Asia and its impact on the south china sea summer monsoon onset. *Front Earth Sci* 8:599447. <https://doi.org/10.3389/feart.2020.599447>
- Yulaeva E, Holton JR, Wallace JM (1994) On the cause of the annual cycle in tropical lower-stratospheric temperatures. *J Atmos Sci* 51(2):169–174. [https://doi.org/10.1175/1520-0469\(1994\)051%3c0169:OTCOTA%3e2.0.CO;2](https://doi.org/10.1175/1520-0469(1994)051%3c0169:OTCOTA%3e2.0.CO;2)
- Zeng QC, Li JP (2002) Interactions between the Northern and Southern hemispheric atmospheres and the essence of monsoon (in Chinese). *Chin J Atmos Sci* 26:433–448. <https://doi.org/10.3878/j.issn.1006-9895.2002.04.01>
- Zhang P, Wu Y, Simpson IR, Smith KL, Callaghan P (2018) A stratospheric pathway linking a colder Siberia to Barents-Kara Sea sea ice loss. *Sci Adv*. <https://doi.org/10.1126/sciadv.aat6025>
- Zhou W, Li C, Wang X (2007) Possible connection between Pacific Oceanic interdecadal pathway and East Asian winter monsoon. *Geophys Res Lett* 34:L01701. <https://doi.org/10.1029/2006GL027809>

**Publisher's Note** Springer Nature remains neutral with regard to jurisdictional claims in published maps and institutional affiliations.

Springer Nature or its licensor (e.g. a society or other partner) holds exclusive rights to this article under a publishing agreement with the author(s) or other rightsholder(s); author self-archiving of the accepted manuscript version of this article is solely governed by the terms of such publishing agreement and applicable law.